Comparisons of a Constrained Least Squares Model versus Human-in-the-loop for Spectral Unmixing to Determine Material Type of GEO Debris[1]

Kira J. Abercromby[(1)], Jason Rapp[(1)], Donald Bedard[(2)], Patrick Seitzer[(3)], Tommaso Cardona[(4)], Heather Cowardin[(5)], Ed Barker[(6)] and Susan Lederer[(7)]

[(1)]*California Polytechnic State University, San Luis Obispo, Aerospace Engineering Department, San Luis Obispo, California, USA, 93407,* kabercro@calpoly.edu

[(2)]*Royal Military College of Canada, Department of Physics, Kingston, Ontario, Canada*

[(3)]*University of Michigan, Astronomy Department, Ann Arbor, MI, USA*

[(4)]*University of Bologna, Bologna, Italy.*

[(5)]*ESCG/Jacobs, Houston, TX, USA*

[(6)]*LZ Technology, Houston, TX USA*

[(7)]*NASA Johnson Space Center, Houston, TX, USA*

ABSTRACT

Spectral reflectance data through the visible regime was collected at Las Campanas Observatory in Chile using an imaging spectrograph on one of the twin 6.5-m Magellan telescopes. The data were obtained on 1-2 May 2012 on the 'Landon Clay' telescope with the LDSS3 (Low Dispersion Survey Spectrograph 3). Five pieces of Geosynchronous Orbit (GEO) or near-GEO debris were identified and observed with an exposure time of 30 seconds on average. In addition, laboratory spectral reflectance data was collected using an Analytical Spectral Device (ASD) field spectrometer at California Polytechnic State University (Cal Poly) in San Luis Obispo on several typical common spacecraft materials including solar cells, circuit boards, various Kapton materials used for multi-layer insulation, and various paints.

The remotely collected data and the laboratory-acquired data were then incorporated in a newly developed model that uses a constrained least squares method to unmix the spectrum in specific material components. The results of this model are compared to the previous method of a human-in-the-loop (considered here the traditional method) that identifies possible material components by varying the materials and percentages until a spectral match is obtained. The traditional model was found to match the remotely collected spectral data after it had been divided by the continuum to remove the space weathering effects, or a "reddening" of the materials. The constrained least-squares model also used the de-reddened spectra as inputs and the results were consistent with those obtained through the traditional method. For comparison, a first-order examination of including reddening effects into the constrained least-squares model will be explored and comparisons to the remotely collected data will be examined. The identification of each object's suspected material component will be discussed herein.

1. Introduction

One of the roles of the NASA's Orbital Debris Program Office at Johnson Space Center (JSC) is to characterize the debris environment by way of assessing the physical properties (type, mass, density, and size) of objects in orbit. Knowledge of the geosynchronous orbit (GEO) debris environment in particular can be used to determine the hazard

[1] This paper includes data gathered with the 6.5 meter Magellan Telescopes located at the Las Campanas Observatory, Chile.

probability at specific GEO altitudes and aid predictions of the future environment. Currently, an optical size is calculated using an assumed albedo for an object and its intensity measurement. However, identification of specific material type or types could improve albedo accuracy and yield a more accurate size estimate for the debris piece. Using spectroscopy, it is possible to determine the surface materials of space objects.

2. Data collection and Reduction

2.1 Telescope Data

The LDSS3 is the Low Dispersion Survey Spectrograph 3 [1]. It has an acquisition field of view of 8.3 arc-minutes diameter. Our observations used a 5 arc-second wide slit, and the VPH-ALL grism. This yields a wavelength range from 3800 to 9000 Angstroms, however we report here only results from 4500 to 8000 Angstroms due to atmospheric refraction effects and the fact that there was no order-separating filter. The spectral sampling was 1.9 Angstroms/CCD pixel. All observations were obtained at airmass < 1.7 to minimize effects of atmospheric refraction [2].

A set of white dwarf standard stars were observed over a range of airmasses to determine atmospheric extinction as a function of wavelength, and set the flux zeropoint. One of the stars was solar analog star SF1615, which is a James Webb Space Telescope (JWST) calibration star [2]. Normally, five 30-second exposures were taken for each object. A more detailed discussion of the procedures used to collect and reduce this data is seen in Seitzer, et al [3].

2.2 Laboratory Data

The laboratory data was collected using an Analytical Spectral Device (ASD) field spectrometer with a resolving power of 10 nanometers at 2 microns with 717 channels. Multiple measurements for each material were obtained to ensure repeatability.

In order to calibrate all laboratory data, a white reference (Spectralon®) is measured to obtain an absolute reflectance measurement. The resulting calibrated spectral data is scaled between zero and one, where a material with nearly zero reflectance would fall close to an absolute reflectance of zero and materials similar to Spectralon would be scaled closer to one. The resulting spectrum is defined as a reflectance factor [4]. However, there is not such an absolute reflectance standard at the same distance and orientation of each of the satellites. Therefore, the data is considered a relative reflectance. In these cases, the shape of the spectrum and the location and strength of the absorption features are used to determine material and not the percent reflectivity. In order to compare measurements from two different objects, it is often necessary to scale to the reflectance so that both objects fit a scaling factor was applied for viewing multiple sets of data on one plot. When this scaling factor was applied, it will be noted. An example of lab data is shown in Figure 1. The data is scaled to the average reflectance between 750 – 800 nm, similar to the other data in this paper.

The materials used for comparison to the lab data were collected mostly at Cal Poly San Luis Obispo. Data was obtained on three cubesats built by three different universities: Montana State, University of Colorado, and Cal Poly. These materials consisted of green and black circuit board, cabling, germanium, aluminum framing, and solar cells of three different types (although the types are unknown to the authors). The solar cells used in the modeling are labeled with the school name that used them to indicate type. Solar cell type TRMM is listed as such due to the serial number on the cell itself. The remaining materials stemmed from a collection of the inertial upperstage (IUS) rocket body. That data consisted of spectra of white paint, cabling, aluminum, multi-layer insulation (MLI) (both the front and the back sides) and valves. There is no material difference between the front and the back of the MLI, however, the back side was less specular due to the stitching on the edges holding the material tighter. Both data sets (the cubesats and the IUS data) were collected in the same fashion with the same spectrometer. The data reduction of the data was also identical.

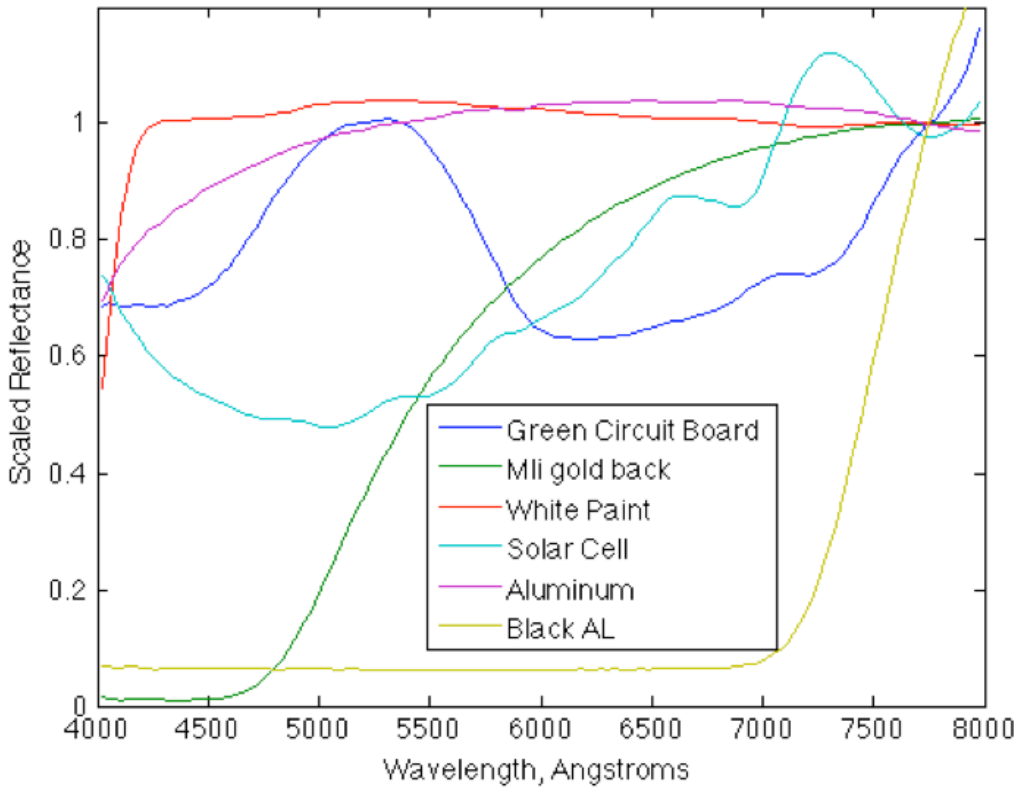

Figure 1: Various reflectance spectra of materials collected in the laboratory. The spectra are normalized to wavelength region of 7500 to 8000 Angstroms.

3. Objects Acquired

The objects acquired on 1-2 May 2012 are shown in Table 1. The objects are five known orbital debris pieces found in the U.S. Space Surveillance Network (SSN) catalog and one Initial Defense Communications Satellite Program (IDCSP) satellite launched in 1967 into an orbit just below GEO. The IDSCP (2655) is a 26-sided structure covered in solar cells of unknown type, but are likely monocrystalline silicon wafers[5]. The cooler cover (29106) prior to launch was covered in MLI with a copper-colored Kapton outer layer [6]. However, it is unknown as to what it looks like now due to the presence of material degradation over time. To the authors knowledge, there is not literature available to indicate what might be on materials in LES DEB (13753) and the two EKRAN 2 debris pieces (12996 and 29014).

Table 1: Objects observed during 1-2 May 2012

SSN	Launch Date	Description
2655	1967	IDSCP
12996	1977	EKRAN 2 DEB
13753	1976	LES 8,9/SOL 11A,B DEB
25000	1968	TITAN TRANSTAGE DEB
29014	1977	EKRAN 2 DEB
29106	2005	MSG 2 DEB (COOLER COVER)

Figure 1 depicts the spectrum of each of the six objects observed, after division by a solar analog (SF1615) spectrum and smoothing. The final spectral resolution was about 10 Angstroms (A). All observations were normalized to 1.0 in the wavelength region from 7500 to 8000 A. The data here is very noisy and difficult to see specific features. These data are single exposure (no co-adding). The authors believe that the fringing from the night sky lines are

causing the noise. The noise makes individual material identification difficult due to the lack of specific absorption features normally used for identification. By examining the shapes of the spectra, it appears that 2655 and 13753 (IDCPS and LES 8/9, respectively) have similar shapes. Objects 29014, 29106, and 12996 (Ekran 2, Cooler Cover, and Ekran 2, respectively) appear to also have similar shapes. Finally object 25000 (Titan Transtage Debris) has a different shape than the other sets of objects. This would indicate that 2655 and 13753 would be composed of similar materials, as would 29014, 29106, and 12996, while 25000 would again be different from the others.

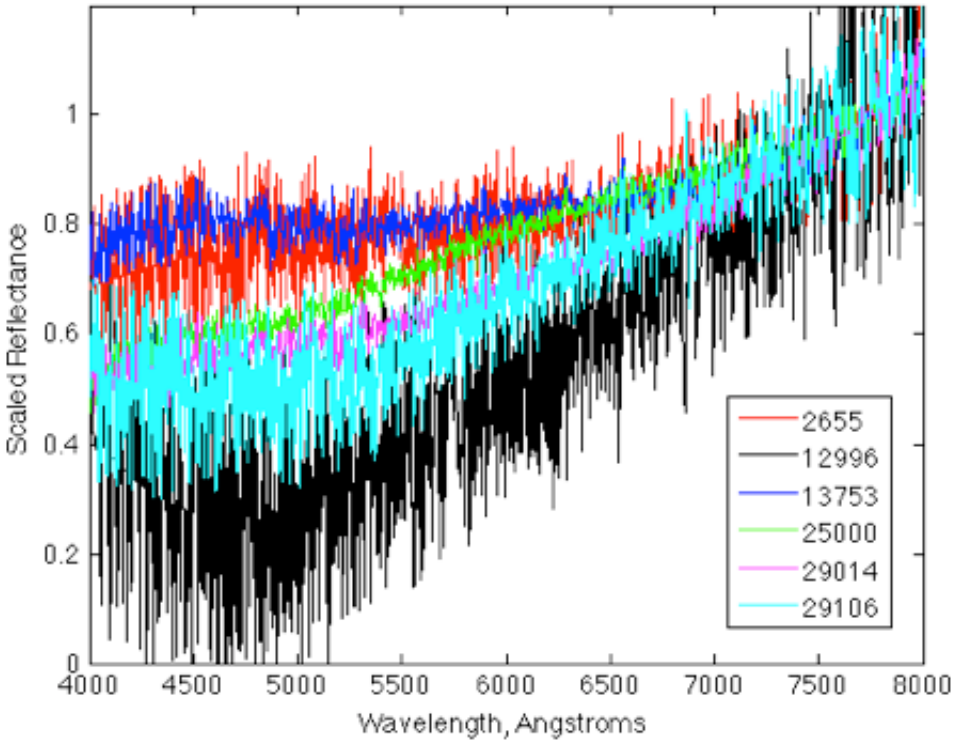

Figure 2: Magellan LDSS3 spectra of six GEO (or near GEO) objects normalized to wavelength region of 7500 to 8000 Angstroms.

4. Model Discussion

4.1 Constrained Linear Least Squares

Spectral unmixing is the process of inverting material proportions from a combined spectrum that has distinct components that are linearly mixed. A constrained least squares solution to the linear unmixing problem was investigated [7].

This leads to spectra adding linearly according to the proportion represented on the surface of the object [8]:

$$S_{combined} = \sum_{i=1}^{n} p_i S_i + N$$

where S is a spectrum, i is an index representing the i^{th} material, p is the material proportion of the full spectrum, and N is noise. This method, however, ignores changes in spectra due to the orientation of both the incident light and orientation of the object. These changes are most significant on the magnitude of the spectrum. The full equation defining the combined spectrum in terms of orientation [8]:

$$S_{combined} = \sum_{i=1}^{n} p_i B_i S_i + N$$

where B_i is the orientation coefficient for the i^{th} material. This equation is still an approximation, however, as the orientation can change the spectrum. The orientation coefficient, B_i, can be determined analytically using [9]:

$$B_i = \frac{dL_r(\vec{\omega}_o)}{E_I(\vec{\omega}_I)\cos\theta_I \, d\vec{\omega}_I}$$

where E_I is the incident irradiance on the vector $\vec{\omega}_I$, θ_I is the angle between ω_I and the surface normal and dL_r is the radiance observed along the vector $\vec{\omega}_o$. L can be calculated using [4]:

$$L = \frac{\Phi}{\Omega A \cos\theta}$$

where Φ is the total radiant flux reflected by the surface, Ω is the angle subtended by the measurement device (in this case the spectrometer probe), A is the area of the surface, and θ is the angle between the surface normal $\vec{N}$ and the $\vec{\omega}_o$ vector.

It should be noted that $S_{combined}$ and S_i can be represented as very long vectors, with reflectance values at each of the measured wavelengths. This allows an expansion into a vector math representation:
$\vec{S}_{combined} = p_1 B_1 \overrightarrow{S_1} + p_2 B_2 \overrightarrow{S_2} + \cdots + p_n B_n \overrightarrow{S_n} + \vec{N}$ where p_i and B_i are both scalars, making it quite easy to restate this as a matrix multiplication problem with a known solution:

$$S_c = SA$$

Unfortunately, the matrix S is not square so it cannot be truly inverted to solve directly for A so a pseudo-inverse can be used. When applied to this problem this inverse is known as a least-squares optimization:

$$S^T S_c = S^T S A$$

Multiplying both sides by S^T creates a square matrix that is guaranteed to be invertible:

$$(S^T S)^{-1} S^T S_c = A$$

This function minimizes the equation and provides a beginning point for the solution to the unmixing problem. Testing this solution, for some combined spectra the unmixer returned negative proportion values, which is physically impossible. This is because the model is trying to match shape and subtracting materials can be the same as adding in terms of the final result. To rectify this issue a constrained least squares function was used, MATLAB's built in `lsqnonneg` function. The function uses a modified Lagrange multiplier method to solve the constrained problem. By reframing this as a vector problem, and recognizing it as a minimization problem, it becomes clear that the Lagrange solution is solving the constrained minimization problem:

$$f = (S_c - SA) \;\; A \geq 0$$

This is solved for the specific $A \geq 0$ case by the `lsqnonneg` function. To maintain the constraint using a Lagrange multiplier method, the function first calculates the least squares solution, including negative solutions. It then uses those solutions to create a vector of logicals defining which solutions are negative, and need to be corrected. This vector becomes the lagrange multiplier, and the optimization is performed. This process is repeated until an optimum solution is found.

To estimate the error in the results when unknown spectra are unmixed, the difference between the original and unmixed spectra is calculated (called the residual). Since a vector approximation method is used to calculate the best unmixing solution, the two-norm is calculated, and used for error:

$$2\,Norm = \sqrt{S^T S}$$

where S is the column vector that contains the reflectance values of the spectrum. This area is then used to calculate the error based on the difference in area.

$$E = \frac{Norm_{diff}}{Norm_{orig}} = \frac{\sqrt{S_{diff}^T S_{diff}}}{\sqrt{S_c^T S_c}}$$

This error estimation gives a percentage error, and gives an estimation of the cut-off point of significant figures in the output [10].

This model takes all the materials supplied and creates the best, combined spectrum based on the above method. There is no human in the loop to include or not include materials based on a prior knowledge.

4.2 Human-in-the-loop (Traditional Method)

The human-in-the-loop or the traditional method has been used in many of the initial results of remotely collected spectral data. The first step is to investigate absorption features, slope, and trend of the spectrum to determine what features might be similar to materials previously seen in the laboratory data. Next, by varying the percentage of each material chosen to match a specific area, a linearly combined spectrum is obtained for comparison to the remotely collected data. Orientation differences between the samples are not taken into account. Validation of this method is accomplished by comparing laboratory data of entire spacecraft to a spectrum created by the traditional method [11].

In order to compare the constrained least squares model with the traditional method, the same materials were used in both methods and those materials were discussed in section 2.2. However, using the traditional method the human in the loop can include any of the materials and not include others due to a prior information or more likely presence or lack there of absorption features. The calculation of the error will be used for both methods and that error is discussed in the section 4.1.

5. Results

5.1 Comparison of the model with the traditional method

In order to compare the constrained linear least squares model to the traditional method, the results for the two objects of known materials, 2655-IDCSP and 29106-cooler cover, are graphically shown in Figure 3 and Figure 4, respectively. In addition to a graphical representation of the modeling, a discussion of whether or not the traditional method agreed with the materials chosen by the constrained least squares model is shown in the table (examples are seen in Table 2 and

Table 3). Notice that not all the materials in the database were used for neither the spectrum created by the constrained linear least squares method nor the traditional method. All objects' material comparisons are shown in their respective tables. One other object was shown graphically (25000, Titan 3C debris) in Figure 5 as example of an object whose materials are not as well known.

The constrained least squares model results for SSN 2655 (IDCSP) are shown in Figure 3 and the materials that were used to make this model are shown in Table 2. The green line is the remotely collected spectrum, the red line is the constrained least squares model spectrum, and the blue line is the difference between the two. The error found for the model for the materials chosen was 7.4%. The calculation of error is discussed in section 4.1 but to reiterate is:

$$E = \frac{Norm_{diff}}{Norm_{orig}} = \frac{\sqrt{S_{diff}^T S_{diff}}}{\sqrt{S_c^T S_c}}$$

where the S_{diff} is the difference between the remotely collected spectrum and the model determined spectrum and S_c is the combined spectrum (or the model determined spectrum). The error is a percent error calculation. For the materials chosen by the model, the error is quite small. Because it is known what the IDCSPs are made of, some of the materials are not likely to be on the spacecraft such as two types of solar cells that were not known to be used on these satellites (e.g. solar cells not yet in production when the IDCSPs were manufactured), multi-types of Kapton, and both green and black circuit board. However, if the model found that the material was present then it was included in the table.

The traditional results are shown in Table 2 as well. Using the same material database as the constrained linear least squares model, materials were combined using linear combination to obtain a spectrum. If this method (deemed the traditional method) found the same material as the constrained linear least squares model, then a yes is

placed in the associated column. Next to the yes is a percentage of that material in the combined spectrum found using the traditional method.

For object 2655, it was found that white paint from Initial Upper Stage (IUS), solar cell MT, and aluminum features and spectrum shapes were present using the traditional method. The rest of the materials determined through the constrained least squares method were not seen by the traditional method. In addition to the materials that were agreed upon or not agreed upon, a percentage of how much of that material was needed to make the linear combination for the traditional method is shown next to the Yes of the specific material. This percentage should not be confused with the percent error, which is listed in the table title. No percentages of specific materials are calculated for the constrained linear least squares method.

The authors believe the solar panels were not oriented in the lab in the same way as they were oriented in space and thus the spectra are greatly varying. Therefore, the constrained least squares model determined the combined spectrum had two types of solar cells where as the traditional method (due to the human in the loop) was able to determine that only one type was likely.

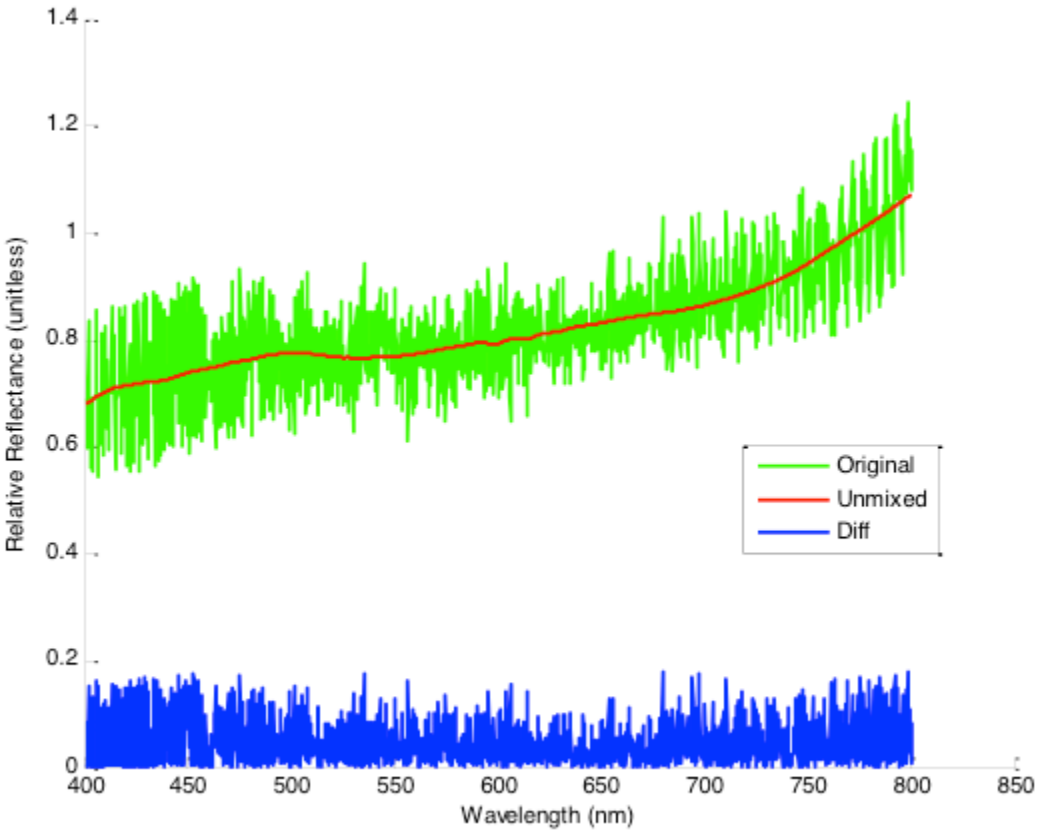

Figure 3: SSN 2655 original data compared with the model data. The error is 7.4% based on the vector norm.

Table 2: A comparison of materials in the methods for SSN 2655

Constrained Linear Least Squares Materials Used in the Combined Spectrum (7.4% error)	**Traditional method materials used in the combined spectrum and percentages (11% error)**
White paint from IUS	Yes (30%)

Blue cable	No
MLI gold	No
Solar Cell TRMM	No
Solar Cell MT	Yes (50%)
Green circuit board	No
Black circuit board	No
AL-Kapton	No
AL Unanodized	Yes (20%)
Germanium	No

The model data overlayed with the remotely collected data for object 29106 (MSG 2 Deb, cooler cover) is seen in Figure 4: SSN 29106 original data compared with the model data. The error is 9.5% based on the vector norm.and the comparison to the traditional method material selection is shown in

. The model error is 9.5% while the traditional method error was 11%. This object is supposed to be an MLI covered cooler cover and so the fact that both methods found solar panels is definitely not correct. However, it is possible that the material in question was not in the laboratory list of those used for the comparison. It was interesting that both methods did find solar panels, however incorrect. This tells the authors that the materials database is missing a bluish type material that was found in most of these samples. The bluish sample could be from many sources such as the solar panels were not taken at the right orientation, all the materials need to be adjusted for orientation and surface roughness, and possibly the material is not in the database. The solar cells are being added in a disproportional amount due to their dark, relatively featureless spectrum. The feature due to Kapton is apart though, seen in Figure 3, as the upturn in reflectance between 500 and 550 nm. The MLI backing is just the back side of MLI. It still has the same copper color, however, it is sewn differently at the edges than the front is sewn giving a slightly different spectral result. Both methods did find Kapton in the remotely collected sample. Specifically, ITO Kapton has a different coating on the exterior lending to a slightly different upturn in the reflectance between 500 and 550 nm.

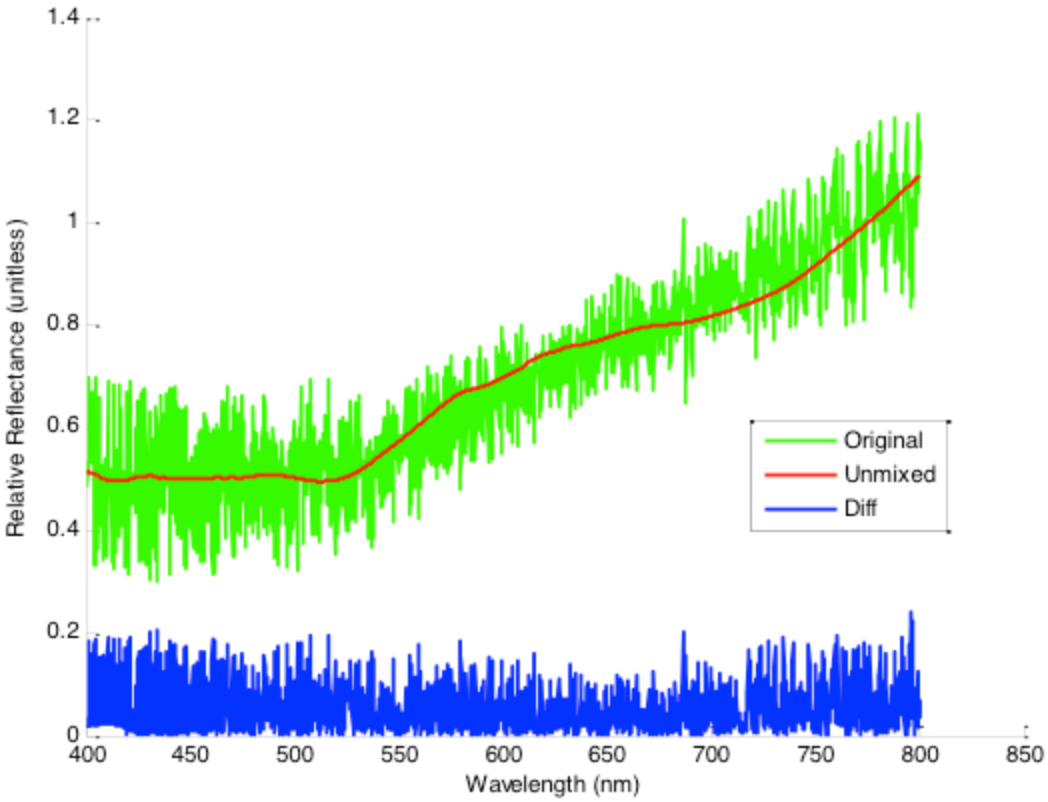

Figure 4: SSN 29106 original data compared with the model data. The error is 9.5% based on the vector norm.

Table 3: A comparison of materials in the methods for SSN 29106

Constrained Linear Least Squares Materials Used in the Combined Spectrum (9.5% error)	**Traditional method materials used in the combined spectrum and percentages (11% error)**
Blue cable	No
MLI gold backing	Yes (30%)
Solar Cell TRMM	Yes (20%)
Solar Cell MT	Yes (40%)
Green circuit board	No
ITO Kapton	No

The model data for SSN 25000 (Titan trans-stage debris) is shown in Figure 5 and the material selection results are shown in Table 4. This sample is particularly interesting due to the removal of solar panels as a possible material. Titan 3C was a rocket body so the fact that both methods did not see solar panels is expect and confirms the models can find the right materials. It was surprising that no white paint was found in the sample through either method, and it is believed the rocket body had some white paint at launch. This indicates that either the orientation the object was in did not allow for the white paint to be observed or the white paint is no longer present. This could be solved

if the spectrum went longer into the infrared where the absorption features due to organic paints are located. If a spectrum including longer in wavelengths were obtained, a strong absorption feature due to Aluminum is seen near 800-850 nm usually appears and would confirm the presence of aluminum. Again the presence of blue cabling suggestions that there is a bluish material that is missing from the dataset.

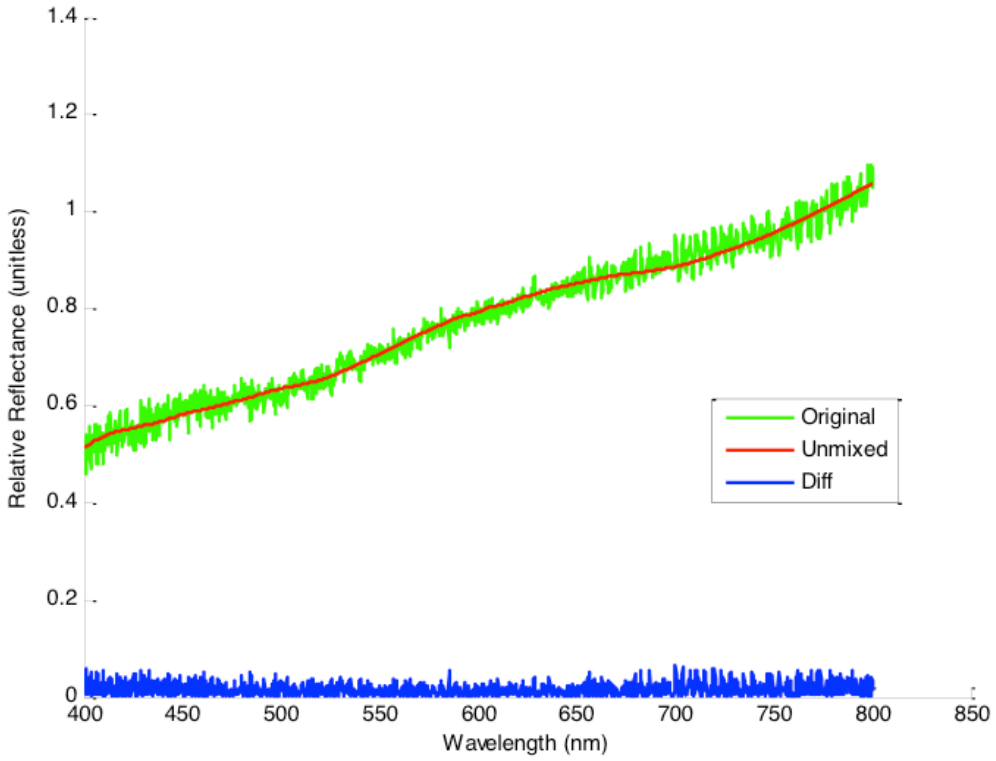

Figure 5: SSN 25000 original data compared with the model data. The error is 2.5% based on the vector norm.

Table 4: A comparison of materials in the methods for SSN 25000

Constrained Linear Least Squares Materials Used in the Combined Spectrum (2.5% error)	**Traditional method materials used in the combined spectrum and percentages (14% error)**
Aluminum	Yes (15%)
Blue cable	Yes (15%)
MLI gold front and back	Yes (25%)
Green circuit board	Yes (15%)
Black board	Yes (10%)
ITO Kapton	Yes (20%)

The rest of the objects are discussed purely by examining their material breakdowns. Object 12996 (Ekran 2 debris) was difficult for both methods to make a guess on the possible material types (shown in Table 5). The percent error for this object was the highest of all six for the constrained least squares method (22 %) and the traditional method (28 %). A large absorption feature was seen centered near 4800 A, but nothing in the database matched the feature in depth thus the error was large for both methods.

Table 5: A comparison of materials in the methods for SSN 12996

Constrained Linear Least Squares Materials Used in the Combined Spectrum (22 % error)	Traditional method materials used in the combined spectrum and percentages (28 % error)
Blue cable	No
Solar Cell MT	Yes (40%)
Green circuit board	Yes (20%)
AL-Kapton	Yes (40%)

The materials matching the spectrum for 13753 (LES 8,9/SOL 11A,B DEB) are shown in Table 6. The errors found between the two methods were approximately equal, 3.2 % and 5% for the constrained linear least squares model and the traditional method respectively, although the model is proving to be more accurate than the traditional using the same materials. However, it is unlikely that this debris piece has this many material types such as the blue cabling and two types of solar panels. The presence of the blue cable shows that there again is missing an item from the database that is bluish in nature and/or that the materials need more attention to the reddening effects.

Table 6: A comparison of materials in the methods for SSN 13753

Constrained Linear Least Squares Materials Used in the Combined Spectrum (3.2 % error)	Traditional method materials used in the combined spectrum and percentages (5% error)
White paint from IUS	Yes (10%)
Blue cable	Yes (10%)
MLI gold back	Yes (10%)
Solar Cell TRMM	Yes (10%)
Solar Cell MT	Yes (10%)
Green circuit board	No
Black circuit board	Yes (10%)
ITO Kapton	Yes (10%)
AL-Kapton	Yes (10%)
Germanium	Yes (20%)

The materials matching the spectrum for 13753 are similar to those found in 29014. (EKRAN 2 DEB). The materials for 29014 are shown in Table 7. The error found with the model was 3.8 % and the traditional method found an equal same error of 5.7%. However, like object 13753 it is unlikely that this debris piece has this many material types such as the blue cabling and two types of solar panels. However, there was good agreement from the two methods showing that again, the model is proving to be more accurate than the traditional with the same materials. The presence of the blue cable shows that there again is missing an item from the database that is bluish in nature or that the materials need more attention to the reddening effects. The model also found two types of Kapton while the traditional method determined that the ITO Kapton gave a slightly better match.

Table 7: A comparison of materials in the methods for SSN 29014

Constrained Linear Least Squares Materials Used in the Combined Spectrum (3.8% error)	Traditional method materials used in the combined spectrum and percentages (5.7% error)
White paint from IUS	No
Blue cable	Yes (10%)
MLI gold backing	Yes (10%)

Solar Cell TRMM	Yes (10%)
Solar Cell MT	Yes (40%)
Green circuit board	Yes (10%)
Black circuit board	No
ITO Kapton	Yes (20%)
AL-Kapton	No

5.2 Division of the continuum

Dividing through the spectrum by the continuum is a method that astronomers have used to determine the material type of a spectrum that is affected by reddening [11]. The idea is to find the slope of the curve and divide the original spectrum by that slope. This method was investigated on the remote spectrum of object 2655 and was used by the constrained least squares model and the traditional method to determine if the division 1) gave different results and 2) if the error improved. This object was chosen due the fact the authors had the most information regarding its preflight material composition. The results are shown in Table 8 and Figure 6. For the model, the error improved from 7.4% to 6.4%. For the traditional method, the error improved from 11% to 9%. The percentages of each material for the traditional method were different from the original breakdown shown in Table 2 and interestingly different solar cell types were also documented. The model found the solar cells used at Cal Poly were a better match, while the traditional found the material to be like a solar cell used on a cubesat from the University of Colorado (CU). The percentages of the various materials were the same but the error did improve.

Table 8: A comparison of materials in the methods for SSN 2655

Constrained Linear Least Squares Materials Used in the Combined Spectrum (6.4% error)	**Traditional method materials used in the combined spectrum and percentages (9% error)**
White paint from IUS	Yes (20%)
Blue cable	No
MLI gold	No
Solar Cell Cal Poly	Yes (60%) but the solar cell from CU
Green circuit board	No
Black circuit board	No
AL-Kapton	No
AL holder	Yes (20%)
Germanium	No

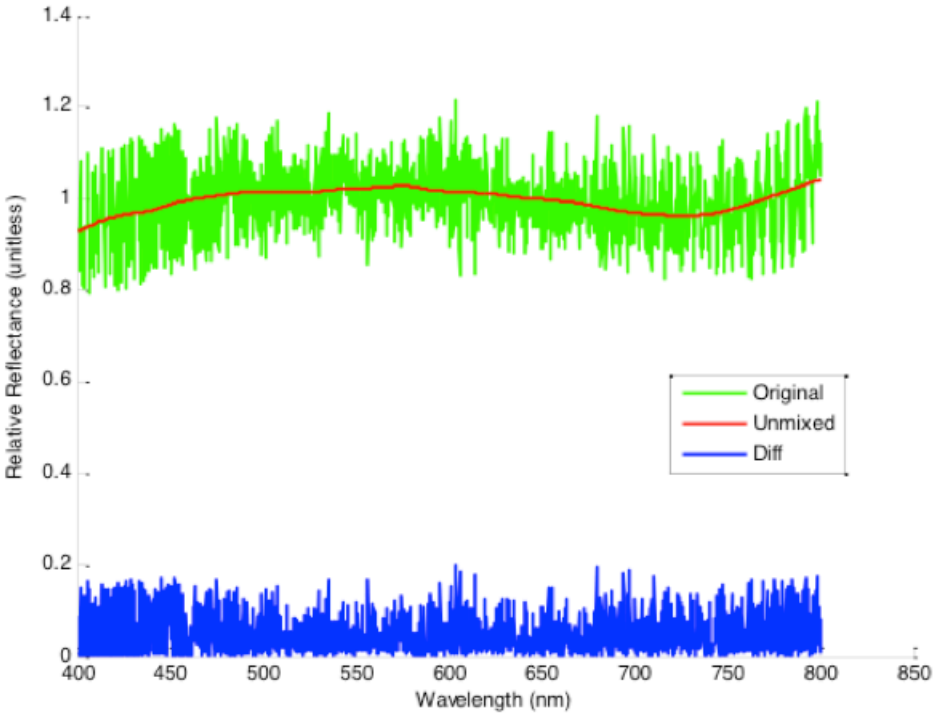

Figure 6: Continuum divided spectrum of 2655 compared to the model and the difference (6.4%) . Please note that the title of original is now the continuum divided spectrum. The unmixed uses the same set of materials for the linear combination.

5.3 Adding in the effect of surface roughness and orientation to the laboratory data

Although the reddening effect previously described appears can be removed from the spectral reflectance measurements of space object, the root cause of this phenomenon remains unknown. Space weathering has been touted as the cause of this effect but the actual physical process that alters, or appears to alter, the reflective properties of the surface material is a mystery.

Laboratory characterization of spacecraft and spacecraft materials [12] as well as modeling experiments [13] have recently shown that the shape of the measured spectral reflectance depends to some degree on the surface roughness of the material as well as in the observational geometry. This is easily reproduced using the reflection model developed by Fresnel in which the magnitude of the ideal specular reflection depends on the index of refraction of the material, $n(\lambda)$, and the angle of incidence, θ_i [14]:

$$R_{total}(\theta_i, \lambda) = \frac{R_{te}(\theta_i, \lambda) + R_{tm}(\theta_i, \lambda)}{2}$$

where R_{te} and R_{tm} are the reflectance for the transverse electric (TE) and transverse magnetic (TM) wave respectively. In cases when the surface is not perfectly smooth, then the material's surface roughness must be taken in consideration and the specular reflectance is reduced and calculated using the following approximation [15]:

$$\rho(\theta, \lambda) \approx R_{total}(\theta_i, \lambda) e^{-(4\pi \frac{\sigma}{\lambda} \cos\theta_i)^2}$$

where σ is the root mean square (rms) surface roughness of the material. The difference $R_{total}(\theta, \lambda) - \rho(\theta, \lambda)$ is the portion of light that is scattered to the remainder of the hemisphere. From the above mathematical relations, Figure 7 and Figure 8 provides spectral reflectance functions for different values of θ_i from an aluminum surface having values of σ equal to 50 nm and 100 nm respectively.

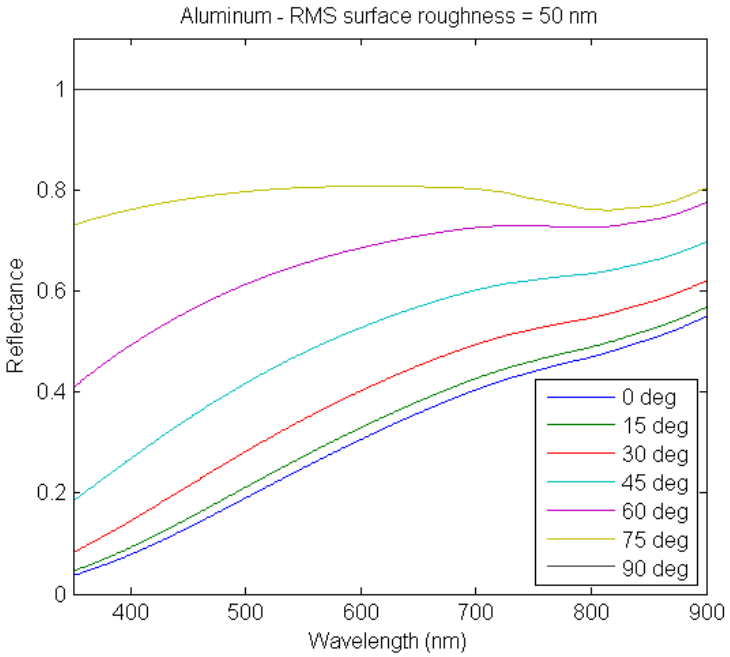

Figure 7. Specular reflection calculated for different values θ_i from an aluminum surface having an rms surface roughness of 50 nm. It is interesting to note that the wide absorption feature which is common to aluminum and centered at approximately 820 nm is very weak for incidence angles below 45°.

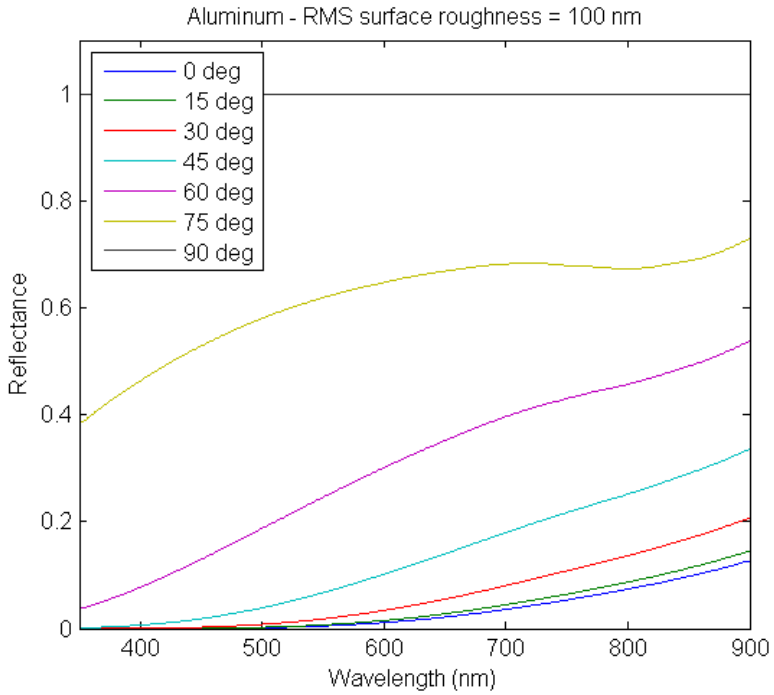

Figure 8. Specular reflection calculated for different values of θ_i from an aluminum surface having an rms surface roughness of 100 nm. In this case, no absorption feature can be seen for incidence angles below 60°.

The first observation from the above figure is that the total amount of energy reflected in the specular direction decreases as the surface roughness increases. Although not shown here, the remainder of the energy is reflected in

the two other reflection components, more specifically, the directional diffuse and diffuse components. Normalizing the reflectance curves illustrated at Figure 7 and Figure 8 to unity, at 700 nm for example, results in a number of curves having very different slopes. Figure 9 illustrates how these curves, taken for the same material whose only difference is the surface roughness and illumination geometry, relate to each other once they have been normalized.

The main point to be taken away from this brief analysis is that a specific material, having a given surface roughness, will show different reflectance curves depending on the illumination geometry. Alternatively, two surfaces composed of the same material with unequal values of surface roughness will show different spectral reflectance curves when taken in the same illumination geometry as discussed in Rodriguez, et al. [16].

Based on these results, future research efforts aimed at identifying material types of space debris will require some consideration of the illumination geometry as well as an on the surface roughness of the materials being compared. With this in mind, work is currently underway to determine how to include these considerations in a reflectance database of materials commonly found on the surfaces of spacecraft as well as the algorithms that are used for the comparative analysis.

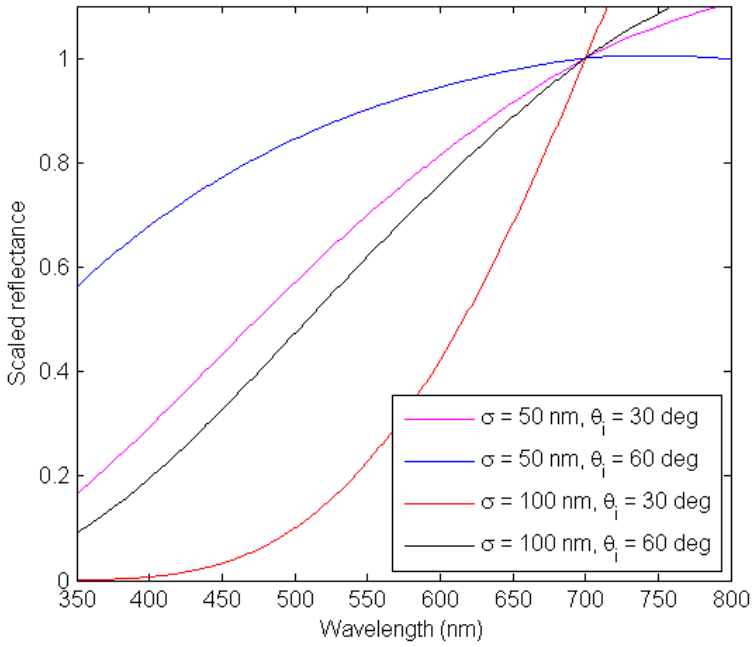

Figure 9. Scaled spectral reflectance functions for an aluminum surfaces with values of σ set to 50 nm and 100 nm taken at two different incidence angles, $\theta_i = 30^o$ and 60^o. The curves have been normalized to unity at 700 nm.

6. Conclusion

The overall conclusion is that the constrained linear least squares method is generally more accurately matches the material composition of these six objects than the traditional method. Overall, the LLS model was 10% closer to the remotely collected data than the traditional method. However, the material selection needs to be expanded to include more materials. The system is missing a bluish type material that was found in most of these samples. The bluish sample could be from many sources such as the solar panels were not taken at the right orientation, all the materials need to be adjusted for orientation and surface roughness, and possibly the material is not in the database. An advantage of using the traditional method is that the percentages of the materials fall out much more easily giving the reader an idea of the structure of the piece.

The need to add in surface roughness and orientation effects on the materials cannot be overstated enough. This method, in order to be used more often, needs better input data in order to make the comparisons. In the future, these adjustments to the model and the input data would need to be made.

However, even with those drawbacks the first cut at using a modeling method to determine material type of remotely collected spectra was successful. In many cases, a first order of magnitude match to the data does indeed indicate the overall composition of the materials. The process is much faster than the traditional method and was more accurate at matching spectral shape and thus, material composition. Using the two methods in conjunction is an improved method to using one method independent of the other. The two methods discussed will continued to be used in conjunction to acquire the best theoretical results for material composition and respective percentages.

7. Acknowledgements

The authors thank the staff at the Las Campanas Observatory for their assistance during the observing.

8. References

1. www.lco.cl/telescopes-information/magellan/instruments/ldss-3
2. Bohlin, R., Flux Calibration Standards for Webb, Space Telescope Institute Newsletter, Winter 2011, page 4.
3. Seitzer, et al., Visible Light Spectroscopy of GEO Debris, Proceedings of 2012 AMOS Technical Conference, Wailea, Maui, Hawaii, 2012.
4. Nicodemus, F. E. (1965). Directional Reflectance and Emissivity of an Opaque Surface. *Applied Optics , 4* (7), 767-773.
5. Lederer, S. M., et al., Characterizing Orbital Debris and Spacecrafts through a Multi-Analytical Approach, Proceedings of 2012 AMOS Technical Conference, Wailea, Maui, Hawaii, 2012.
6. Jah, M., and Kelecy, T., Studies of the Orbit of the MSG 2 Cooler Cover, IAC 2010.
7. Jason's thesis
8. Keshava, N., & and Mustard, J. F. (2002). Spectral Unmixing. *IEEE Signal Processing Magazine* (January 2002), 44-57.
9. Griffiths. (1999). *Introduction to Electrodynamics, 3rd Edition.* Upper Saddle River, New Jersey: Prentice-Hall.
10. Strang, G. (2007). *Computational Science and Engineering.* Wellesley: Wellesley-Cambridge Press.
11. Jorgensen, K., Okada, J, Bradford, L, Hall, D, Africano, J., Hamada, K., Sydney, P., Stansbery, E., and Kervin, P. (2003), Obtaining Material Type of Orbiting Objects through Reflectance Spectroscopy Measurements, Proceedings of 2003 AMOS Technical Conference, Wailea, Maui, Hawaii, 2003.
12. Bédard, D., Lévesque, M., & Wallace, B. (2011). Spectral BRDF measurement of small satellites in Canada. *2011 AMOS Technical Conference.* Kihei, Maui, HI: The Maui Economic Develpment Board.
13. Bedard, D. (2011). Using a physics-based reflection model to study the reddening effect observed in spectrometric measurements of artificial space objects. *2011 AMOS Technical Conference.* Kihei, Maui, HI: The Maui Economic Development Board.
14. Pedrotti, F. L., Pedrotti, L. S., & Pedrotti, L. M. (2007). *Introduction to Optics. 3rd ed.* Uper Saddle River, NJ 07458: Pearson Prentice Hall.
15. Westin, S. H., Hongsong, L., & Torrance, K. E. (2004). A comparison of four BRDF models. In H. Jensen, & A. Keller (Ed.). (pp. 1-10). Eurographics Symposium on Rendering.
16. Rodriguez, H., Abercromby, K.J., Mulrooney, M, and Barker,E (2007). Optrical Properties of Multi-layered Insulation, Proceedings of 2007 AMOS Technical Conference, Wailea, Maui, Hawaii, 2007.